

# Binary Linear Classification and Feature Selection via Generalized Approximate Message Passing

Justin Ziniel and Philip Schniter

**Abstract**—For the problem of binary linear classification and feature selection, we propose algorithmic approaches to classifier design based on the generalized approximate message passing (GAMP) algorithm, recently proposed in the context of compressive sensing. Our work focuses on the regime where the number of features greatly exceeds the number of training examples, but where only a few features suffice for accurate classification. We show that sum-product GAMP can be used to (approximately) minimize the classification error rate and max-sum GAMP can be used to minimize a wide variety of regularized loss functions. Moreover, we show how a “turbo” extension to GAMP allows us to learn weight vectors that exhibit structured sparsity. Furthermore, we describe an expectation-maximization (EM)-based scheme to learn the associated model parameters online, as an alternative to cross-validation, and we show that GAMPs state evolution framework can be used to accurately predict the misclassification rate. Finally, we present a detailed numerical study to confirm the accuracy, speed, and flexibility afforded by our GAMP-based approaches to binary linear classification.

## I. INTRODUCTION

In this work we consider binary linear classification and feature selection [1]. The objective of *binary linear classification* is to learn the weight vector  $\mathbf{w} \in \mathbb{R}^N$  that best predicts an unknown binary class label  $y \in \{-1, 1\}$  associated with a given vector of quantifiable features  $\mathbf{x} \in \mathbb{R}^N$  from the sign of a linear “score”  $z \triangleq \langle \mathbf{x}, \mathbf{w} \rangle$ .<sup>1</sup> The goal of *linear feature selection* is to identify which subset of the  $N$  weights in  $\mathbf{w}$  are necessary for accurate prediction of the unknown class label  $y$ , since in some applications (e.g., multi-voxel pattern analysis) this subset itself is of primary concern.

In formulating this linear feature selection problem, we assume that there exists a  $K$ -sparse weight vector  $\mathbf{w}$  (i.e.,  $\|\mathbf{w}\|_0 = K \ll N$ ) such that  $y = \text{sgn}(\langle \mathbf{x}, \mathbf{w} \rangle - \mathbf{e})$ , where  $\text{sgn}(\cdot)$  is the signum function and  $\mathbf{e} \sim p_{\mathbf{e}}$  is a random perturbation accounting for model inaccuracies. For the purpose of learning  $\mathbf{w}$ , we assume the availability of  $M$  labeled training examples generated independently according to this model:

$$y_m = \text{sgn}(\langle \mathbf{x}_m, \mathbf{w} \rangle - \mathbf{e}_m), \quad \forall m = 1, \dots, M, \quad (1)$$

Ziniel and Schniter are with the Dept. of Electrical and Computer Engineering, The Ohio State University, Columbus, Ohio; e-mail: {zinielj, schniter}@ece.osu.edu. Their work on this project has been supported by NSF grant CCF-1218754, by NSF grant CCF-1018368, and by DARPA/ONR grant N66001-10-1-4090.

Portions of this work were presented in Feb. 2013 at the Workshop on Information Theory and its Applications in San Diego, CA.

<sup>1</sup>We note that one could also compute the score from a fixed non-linear transformation  $\psi(\cdot)$  of the original feature  $\mathbf{x}$  via  $z \triangleq \langle \psi(\mathbf{x}), \mathbf{w} \rangle$  as in kernel-based classification. Although the methods we describe here are directly compatible with this approach, we write  $z = \langle \mathbf{x}, \mathbf{w} \rangle$  for simplicity.

with  $\mathbf{e}_m \sim \text{i.i.d } p_{\mathbf{e}}$ . It is common to express the relationship between the label  $y_m$  and the score  $z_m \triangleq \langle \mathbf{x}_m, \mathbf{w} \rangle$  in (1) via the conditional pdf  $p_{y_m|z_m}(y_m|z_m)$ , known as the “activation function,” which can be related to the perturbation pdf  $p_{\mathbf{e}}$  via

$$p_{y_m|z_m}(1|z_m) = \int_{-\infty}^{z_m} p_{\mathbf{e}}(e) de = 1 - p_{y_m|z_m}(-1|z_m). \quad (2)$$

We are particularly interested in classification problems in which the number of potentially discriminatory features  $N$  drastically exceeds the number of available training examples  $M$ . Such computationally challenging problems are of great interest in a number of modern applications, including text classification [2], multi-voxel pattern analysis (MVPA) [3]–[5], conjoint analysis [6], and microarray gene expression [7]. In MVPA, for instance, neuroscientists attempt to infer which regions in the human brain are responsible for distinguishing between two cognitive states by measuring neural activity via fMRI at  $N \approx 10^4$  voxels. Due to the expensive and time-consuming nature of working with human subjects, classifiers are routinely trained using only  $M \approx 10^2$  training examples, and thus  $N \gg M$ .

In the  $N \gg M$  regime, the model of (1) coincides with that of *noisy one-bit compressed sensing* (CS) [8], [9]. In that setting, it is typical to write (1) in matrix-vector form using  $\mathbf{y} \triangleq [y_1, \dots, y_M]^T$ ,  $\mathbf{e} \triangleq [\mathbf{e}_1, \dots, \mathbf{e}_M]^T$ ,  $\mathbf{X} \triangleq [\mathbf{x}_1, \dots, \mathbf{x}_M]^T$ , and elementwise  $\text{sgn}(\cdot)$ , yielding

$$\mathbf{y} = \text{sgn}(\mathbf{X}\mathbf{w} - \mathbf{e}), \quad (3)$$

where  $\mathbf{w}$  embodies the signal-of-interest’s sparse representation,  $\mathbf{X} = \Phi\Psi$  is a concatenation of a linear measurement operator  $\Phi$  and a sparsifying signal dictionary  $\Psi$ , and  $\mathbf{e}$  is additive noise.<sup>2</sup> Importantly, in the  $N \gg M$  setting, [9] established performance guarantees on the estimation of  $K$ -sparse  $\mathbf{w}$  from  $O(K \log N/K)$  binary measurements of the form (3), under i.i.d Gaussian  $\{\mathbf{x}_m\}$  and mild conditions on the perturbation process  $\{\mathbf{e}_m\}$ , even when the entries within  $\mathbf{x}_m$  are correlated. This result implies that, in large binary linear classification problems, accurate feature selection is indeed possible from  $M \ll N$  training examples, as long as the underlying weight vector  $\mathbf{w}$  is sufficiently sparse. Not surprisingly, many techniques have been proposed to find such weight vectors [10]–[17].

In addition to theoretical analyses, the CS literature also offers a number of high-performance algorithms for the inference of  $\mathbf{w}$  in (3). Thus, the question arises as to whether

<sup>2</sup>For example, the common case of additive white Gaussian noise (AWGN)  $\{\mathbf{e}_m\} \sim \text{i.i.d } \mathcal{N}(0, v)$  corresponds to the “probit” activation function, i.e.,  $p_{y_m|z_m}(1|z_m) = \Phi(z_m/v)$ , where  $\Phi(\cdot)$  is the standard-normal cdf.

these algorithms also show advantages in the domain of binary linear classification and feature selection. In this paper, we answer this question in the affirmative by focusing on the *generalized approximate message passing* (GAMP) algorithm [18], which extends the AMP algorithm [19], [20] from the case of linear, AWGN-corrupted observations (i.e.,  $\mathbf{y} = \mathbf{X}\mathbf{w} - \mathbf{e}$  for  $\mathbf{e} \sim \mathcal{N}(\mathbf{0}, v\mathbf{I})$ ) to the case of generalized-linear observations, such as (3). AMP and GAMP are attractive for several reasons: (i) For i.i.d sub-Gaussian  $\mathbf{X}$  in the large-system limit (i.e.,  $M, N \rightarrow \infty$  with fixed ratio  $\delta = \frac{M}{N}$ ), they are rigorously characterized by a state-evolution whose fixed points, when unique, are optimal [21]; (ii) Their state-evolutions predict very fast runtimes due to mean-squared error (MSE) that decays exponentially with iteration  $k$  (i.e.,  $\text{MSE}(k) \leq e^{-bk}\text{MSE}(0)$  for some  $b > 0$ ) and per-iteration complexity of only  $O(MN)$ ; (iii) They are very flexible with regard to data-modeling assumptions (see, e.g., [22]); (iv) Their assumed model parameters can be learned online using an expectation-maximization (EM) approach that has been shown to yield state-of-the-art mean-squared reconstruction error in CS problems [23].

In this work, we develop a GAMP-based approach to binary linear classification and feature selection that makes the following contributions: 1) in Section II, we show that GAMP implements a particular approximation to the error-rate minimizing linear classifier under the assumed model (1); 2) in Section III, we show that GAMP's state evolution framework can be used to characterize the misclassification rate in the large-system limit; 3) in Section IV, we develop methods to implement logistic, probit, and hinge-loss-based regression using both max-sum and sum-product versions of GAMP, and we further develop a method to make these classifiers robust in the face of corrupted training labels; 4) in Section V, we present an EM-based scheme to learn the model parameters online, as an alternative to cross-validation; and 5) in Section VI, we illustrate how a “turbo” extension to GAMP allows us to learn weight vectors that exhibit structured sparsity (e.g., feature selection with spatially clustered features). The numerical study presented in Section VII then confirms the efficacy, flexibility, and speed afforded by our GAMP-based approaches to binary classification.

*Notation:* Random quantities are typeset in sans-serif (e.g.,  $\mathbf{e}$ ) while deterministic quantities are typeset in serif (e.g.,  $e$ ). The pdf of random variable  $\mathbf{e}$  under deterministic parameters  $\theta$  is written as  $p_{\mathbf{e}}(e; \theta)$ , where the subscript is sometimes omitted when the meaning is clear. Column vectors are typeset in boldface lower-case (e.g.,  $\mathbf{y}$  or  $\mathbf{y}$ ), matrices in boldface uppercase (e.g.,  $\mathbf{X}$  or  $\mathbf{X}$ ), and their transpose is denoted by  $(\cdot)^\top$ . For vector  $\mathbf{y} = [y_1, \dots, y_M]^\top$ ,  $\mathbf{y}_{m:n}$  refers to the subvector  $[y_m, \dots, y_n]^\top$ . Finally,  $\mathcal{N}(\mathbf{a}; \mathbf{b}, \mathbf{C})$  is the multivariate normal distribution, a function of the vector  $\mathbf{a}$ , with mean  $\mathbf{b}$  and covariance matrix  $\mathbf{C}$ , while  $\phi(\cdot)$  and  $\Phi(\cdot)$  denote the standard normal pdf and cdf, respectively.

## II. GAMP FOR CLASSIFICATION

In this section, we introduce generalized approximate message passing (GAMP) from the perspective of binary linear

classification. In particular, we show that the *sum-product* variant of GAMP is a loopy belief propagation (LBP) approximation of the classification-error-rate minimizing linear classifier and that the *max-sum* variant of GAMP is a LBP implementation of the standard regularized-loss-minimization approach to linear classifier design.

### A. Sum-Product GAMP

Suppose that we are given  $M$  labeled training examples  $\{\mathbf{y}_m, \mathbf{x}_m\}_{m=1}^M$ , and  $T$  test feature vectors  $\{\mathbf{x}_t\}_{t=M+1}^{M+T}$  associated with unknown test labels  $\{\mathbf{y}_t\}_{t=M+1}^{M+T}$ , all obeying the noisy linear model (1) under some known error pdf  $p_{\mathbf{e}}$ , and thus known  $p_{\mathbf{y}_m|\mathbf{z}_m}$ . We then consider the problem of computing the classification-error-rate minimizing hypotheses  $\{\hat{\mathbf{y}}_t\}_{t=M+1}^{M+T}$ ,

$$\hat{\mathbf{y}}_t = \arg \max_{y_t \in \{-1, 1\}} p_{\mathbf{y}_t|\mathbf{y}_{1:M}}(y_t | \mathbf{y}_{1:M}; \mathbf{X}), \quad (4)$$

with  $\mathbf{y}_{1:M} \triangleq [y_1, \dots, y_M]^\top$  and  $\mathbf{X} \triangleq [\mathbf{x}_1, \dots, \mathbf{x}_{M+T}]^\top$ . Note that we treat the labels  $\{\mathbf{y}_m\}_{m=1}^{M+T}$  as random but the features  $\{\mathbf{x}_m\}_{m=1}^{M+T}$  as deterministic parameters. The probabilities in (4) can be computed via the marginalization

$$p_{\mathbf{y}_t|\mathbf{y}_{1:M}}(y_t | \mathbf{y}_{1:M}; \mathbf{X}) = p_{\mathbf{y}_t, \mathbf{y}_{1:M}}(y_t, \mathbf{y}_{1:M}; \mathbf{X}) C_{\mathbf{y}}^{-1} \quad (5)$$

$$= C_{\mathbf{y}}^{-1} \sum_{\mathbf{y} \in \mathcal{Y}_t(y_t)} \int p_{\mathbf{y}, \mathbf{w}}(\mathbf{y}, \mathbf{w}; \mathbf{X}) d\mathbf{w} \quad (6)$$

with scaling constant  $C_{\mathbf{y}} \triangleq p_{\mathbf{y}_{1:M}}(\mathbf{y}_{1:M}; \mathbf{X})$ , label vector  $\mathbf{y} = [y_1, \dots, y_{M+T}]^\top$ , and constraint set  $\mathcal{Y}_t(y) \triangleq \{\tilde{\mathbf{y}} \in \{-1, 1\}^{M+T} \text{ s.t. } [\tilde{\mathbf{y}}]_t = y \text{ and } [\tilde{\mathbf{y}}]_m = y_m \forall m = 1, \dots, M\}$  which fixes the  $t$ th element of  $\mathbf{y}$  at the value  $y$  and the first  $M$  elements of  $\mathbf{y}$  at the values of the corresponding training labels. The joint pdf in (6) factors as

$$p_{\mathbf{y}, \mathbf{w}}(\mathbf{y}, \mathbf{w}; \mathbf{X}) = \prod_{m=1}^{M+T} p_{\mathbf{y}_m|\mathbf{z}_m}(y_m | \mathbf{x}_m^\top \mathbf{w}) \prod_{n=1}^N p_{\mathbf{w}_n}(w_n) \quad (7)$$

due to the model (1) and assuming a separable prior, i.e.,

$$p_{\mathbf{w}}(\mathbf{w}) = \prod_{n=1}^N p_{\mathbf{w}_n}(w_n). \quad (8)$$

We will relax the separability assumption (8) in Section VI.

The factorization (7) is illustrated using the *factor graph* in Fig. 1a, which connects the various random variables to the pdf factors in which they appear. Although exact computation of the marginal posterior test-label probabilities via (6) is computationally intractable due to the high-dimensional summation and integration, the factor graph in Fig. 1a suggests the use of loopy belief propagation (LBP) [24], and in particular the *sum-product algorithm* (SPA) [25], as a tractable way to approximate these marginal probabilities. Although the SPA guarantees exact marginal posteriors only under non-loopy (i.e., tree-structured graphs), it has proven successful in many applications with loopy graphs, such as turbo decoding [26], computer vision [27], and compressive sensing [18]–[20].

Because a direct application of the SPA to the factor graph in Fig. 1a is itself computationally infeasible in the high-dimensional case of interest, we turn to a recently developed

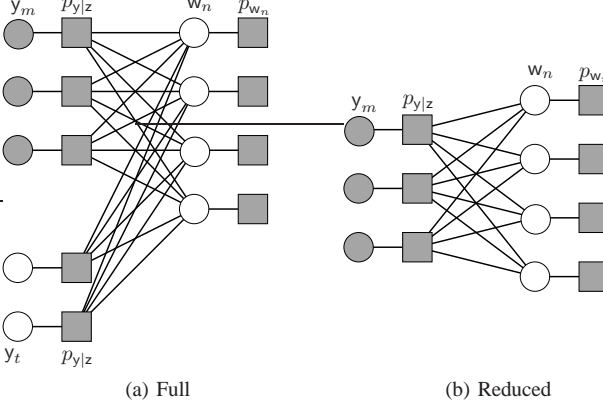


Fig. 1: Factor graph representations of the integrand of (7), with white/grey circles denoting unobserved/observed random variables, and rectangles denoting pdf ‘‘factors’’.

approximation: the sum-product variant of GAMP [18], as specified in Algorithm 1. The GAMP algorithm is specified in Algorithm 1 for a given instantiation of  $\mathbf{X}$ ,  $p_{y|z}$ , and  $\{p_{w_n}\}$ . There, the expectation and variance in lines 5-6 and 16-17 are taken elementwise w.r.t the GAMP-approximated marginal posterior pdfs (with superscript  $k$  denoting the iteration)

$$q(z_m | \hat{p}_m, \tau_{p_m}^k) = p_{y_m|z_m}(y_m | z_m) \mathcal{N}(z_m; \hat{p}_m^k, \tau_{p_m}^k) C_z^{-1} \quad (9)$$

$$q(w_n | \hat{r}_n^k, \tau_r^k) = p_{w_n}(w_n) \mathcal{N}(w_n; \hat{r}_n^k, \tau_r^k) C_w^{-1} \quad (10)$$

with appropriate normalizations  $C_z$  and  $C_w$ , and the vector-vector multiplications and divisions in lines 3, 9, 11, 12, 14, 13, 20 are performed elementwise. Due to space limitations, we refer the interested reader to [18] for an overview and derivation of GAMP, to [21] for rigorous analysis under large i.i.d sub-Gaussian  $\mathbf{X}$ , and to [28] for fixed-point analysis under arbitrary  $\mathbf{X}$ .

Applying GAMP to the classification factor graph in Fig. 1a and examining the resulting form of lines 5-6 in Algorithm 1, it becomes evident that the test-label nodes  $\{y_t\}_{t=M+1}^{M+T}$  do not affect the GAMP weight estimates  $(\hat{w}^k, \tau_w^k)$  and thus the factor graph can effectively be simplified to the form shown in Fig. 1b, after which the (approximated) posterior test-label pdfs are computed via

$$p_{y_t|y_{1:M}}(y_t | \mathbf{y}_{1:M}; \mathbf{X}) \approx \int p_{y_t|z_t}(y_t | z_t) \mathcal{N}(z_t; \hat{z}_t^\infty, \tau_{z,t}^\infty) dz_t \quad (11)$$

where  $\hat{z}_t^\infty$  and  $\tau_{z,t}^\infty$  denote the  $t^{th}$  element of the GAMP vectors  $\hat{z}^k$  and  $\tau_z^k$ , respectively, at the final iteration ‘‘ $k = \infty$ ’’.

### B. Max-Sum GAMP

An alternate approach to linear classifier design is through the minimization of a regularized loss function, e.g.,

$$\hat{w} = \arg \min_{\mathbf{w} \in \mathbb{R}^N} \sum_{m=1}^M f_{z_m}(\mathbf{x}_m^\top \mathbf{w}) + \sum_{n=1}^N f_{w_n}(w_n), \quad (12)$$

where  $f_{z_m}(\cdot)$  are  $y_m$ -dependent convex loss functions (e.g., logistic, probit, or hinge based) and where  $f_{w_n}(\cdot)$  are convex regularization terms (e.g.,  $f_{w_n}(w) = \lambda w^2$  for  $\ell_2$  regularization and  $f_{w_n}(w) = \lambda |w|$  for  $\ell_1$  regularization).

---

### Algorithm 1 Generalized Approximate Message Passing

---

**Input:** Matrix  $\mathbf{X}$ , priors  $p_{w_n}(\cdot)$ , activation functions  $p_{y_m|z_m}(y_m | \cdot)$ , and mode  $\in \{\text{SumProduct}, \text{MaxSum}\}$   
**Initialize:**  $k \leftarrow 0$ ;  $\hat{s}^{-1} \leftarrow \mathbf{0}$ ;  $\mathbf{S} \leftarrow |\mathbf{X}|^2$ ;  $\hat{\mathbf{w}}^0 \leftarrow \mathbf{0}$ ;  $\tau_w^0 \leftarrow 1$

- 1: **repeat**
- 2:    $\tau_p^k \leftarrow \mathbf{S} \tau_w^k$
- 3:    $\hat{\mathbf{p}}^k \leftarrow \mathbf{X} \hat{\mathbf{w}}^k - \hat{s}^{k-1} \tau_p^k$
- 4:   **if** SumProduct **then**
- 5:      $\hat{z}^k \leftarrow \mathbb{E}\{\mathbf{z} | \hat{\mathbf{p}}^k, \tau_p^k\}$
- 6:      $\tau_z^k \leftarrow \text{var}\{\mathbf{z} | \hat{\mathbf{p}}^k, \tau_p^k\}$
- 7:   **else if** MaxSum **then**
- 8:      $\hat{z}^k \leftarrow \text{prox}_{\tau_p^k f_{z_m}}(\hat{\mathbf{p}}^k)$
- 9:      $\tau_z^k \leftarrow \tau_p^k \text{prox}'_{\tau_p^k f_{z_m}}(\hat{\mathbf{p}}^k)$
- 10:   **end if**
- 11:    $\tau_s^k \leftarrow 1/\tau_p^k - \tau_z^k/(\tau_p^k)^2$
- 12:    $\hat{s}^k \leftarrow (\hat{z}^k - \hat{\mathbf{p}}^k)/\tau_p^k$
- 13:    $\tau_r^k \leftarrow 1/(\mathbf{S}^\top \tau_s^k)$
- 14:    $\hat{\mathbf{r}}^k \leftarrow \hat{\mathbf{w}}^k + \tau_r^k \mathbf{X}^\top \hat{s}^k$
- 15:   **if** SumProduct **then**
- 16:      $\hat{\mathbf{w}}^{k+1} \leftarrow \mathbb{E}\{\mathbf{w} | \hat{\mathbf{r}}^k, \tau_r^k\}$
- 17:      $\tau_w^{k+1} \leftarrow \text{var}\{\mathbf{w} | \hat{\mathbf{r}}^k, \tau_r^k\}$
- 18:   **else if** MaxSum **then**
- 19:      $\hat{\mathbf{w}}^{k+1} \leftarrow \text{prox}_{\tau_r^k f_{w_n}}(\hat{\mathbf{r}}^k)$
- 20:      $\tau_w^{k+1} \leftarrow \tau_r^k \text{prox}'_{\tau_r^k f_{w_n}}(\hat{\mathbf{r}}^k)$
- 21:   **end if**
- 22:    $k \leftarrow k + 1$
- 23: **until** Terminated

---

The solution to (12) can be recognized as the *maximum a posteriori* (MAP) estimate of random vector  $\mathbf{w}$  given a separable prior  $p_{\mathbf{w}}(\cdot)$  and likelihood corresponding to (1), i.e.,

$$p_{\mathbf{y}|\mathbf{w}}(\mathbf{y} | \mathbf{w}; \mathbf{X}) = \prod_{m=1}^M p_{y_m|z_m}(y_m | \mathbf{x}_m^\top \mathbf{w}), \quad (13)$$

when  $f_{z_m}(z) = -\log p_{y_m|z_m}(y_m | z)$  and  $f_{w_n}(w) = -\log p_{w_n}(w)$ . Importantly, this statistical model is exactly the one yielding the reduced factor graph in Fig. 1b.

Similar to how sum-product LBP can be used to compute (approximate) marginal posteriors in loopy graphs, max-sum LBP can be used to compute the MAP estimate [29]. Since max-sum LBP is itself intractable for the high-dimensional problems of interest, we turn to the max-sum variant of GAMP [18], which is also specified in Algorithm 1. There, lines 8-9 are to be interpreted as

$$\hat{z}_m^k = \text{prox}_{\tau_{p_m}^k f_{z_m}}(\hat{p}_m^k), \quad m = 1, \dots, M, \quad (14)$$

$$\tau_{z_m}^k = \tau_{p_m}^k \text{prox}'_{\tau_{p_m}^k f_{z_m}}(\hat{p}_m^k), \quad m = 1, \dots, M, \quad (15)$$

with  $(\cdot)'$  and  $(\cdot)''$  denoting first and second derivatives and

$$\text{prox}_{\tau_f}(v) \triangleq \arg \min_{u \in \mathbb{R}} \left[ f(u) + \frac{1}{2\tau}(u - v)^2 \right] \quad (16)$$

$$\text{prox}'_{\tau_f}(v) = (1 + \tau f''(\text{prox}_{\tau_f}(v)))^{-1}, \quad (17)$$

and lines 19–20 are to be interpreted similarly. It is known [28] that, for *arbitrary*  $\mathbf{X}$ , the fixed points of GAMP correspond to the critical points of the optimization objective (12).

### C. GAMP Summary

In summary, the sum-product and max-sum variants of the GAMP algorithm provide tractable methods of approximating the posterior test-label probabilities  $\{p_{y_t|\mathbf{y}_{1:M}}(y_t|\mathbf{y}_{1:M})\}_{t=T+1}^{M+T}$  and finding the MAP weight vector  $\hat{\mathbf{w}} = \arg \max_{\mathbf{w}} p_{\mathbf{w}|\mathbf{y}_{1:M}}(\mathbf{w}|\mathbf{y}_{1:M})$ , respectively, under the label-generation model (13) [equivalently, (1)] and the separable weight-vector prior (8), assuming that the distributions  $p_{y|z}$  and  $\{p_{\mathbf{w}_n}\}$  are known and facilitate tractable scalar-nonlinear update steps 5–6, 8–9, 16–17, and 19–20. In Section IV, we discuss the implementation of these update steps for several popular activation functions; in Section V, we discuss how the parameters of  $p_{y_m|z_m}$  and  $p_{\mathbf{w}_n}$  can be learned online; and in Section VI, we discuss extensions to the case of non-separable weight-vector priors  $p_{\mathbf{w}}$ .

## III. MISCLASSIFICATION RATE VIA STATE EVOLUTION

As mentioned earlier, the behavior of GAMP in the large-system limit (i.e.,  $M, N \rightarrow \infty$  with fixed ratio  $\delta = \frac{M}{N}$ ) under i.i.d sub-Gaussian  $\mathbf{X}$  is characterized by a scalar state evolution [18], [21]. We now describe how this state evolution can be used to characterize the test-error rate of the linear-classification GAMP algorithms described in Section II.

The GAMP state evolution characterizes average GAMP performance over an ensemble of (infinitely sized) problems, each associated with one realization  $(\mathbf{y}, \mathbf{X}, \mathbf{w})$  of the random triple  $(\mathbf{y}, \mathbf{X}, \mathbf{w})$ . Recall that, for a given problem realization  $(\mathbf{y}, \mathbf{X}, \mathbf{w})$ , the GAMP iterations in Algorithm 1 yields the sequence of estimates  $\{\hat{\mathbf{w}}^k\}_{k=1}^{\infty}$  of the true weight vector  $\mathbf{w}$ . Then, according to the state evolution,  $p_{\mathbf{w}, \hat{\mathbf{w}}^k}(\mathbf{w}, \hat{\mathbf{w}}^k) \sim \prod_n p_{\mathbf{w}_n, \hat{\mathbf{w}}_n^k}(\mathbf{w}_n, \hat{\mathbf{w}}_n^k)$  and the first two moments of the joint pdf  $p_{\mathbf{w}_n, \hat{\mathbf{w}}_n^k}$  can be computed using [18, Algorithm 3].

Suppose that the  $(\mathbf{y}, \mathbf{X})$  above represent training examples associated with a true weight vector  $\mathbf{w}$ , and that  $(\mathbf{y}, \mathbf{x})$  represents a test pair also associated with the same  $\mathbf{w}$  and with  $\mathbf{x}$  having i.i.d elements distributed identically to those of  $\mathbf{X}$  (with, say, variance  $\frac{1}{M}$ ). The true and iteration- $k$ -estimated test scores are then  $\mathbf{z} \triangleq \mathbf{x}^T \mathbf{w}$  and  $\hat{\mathbf{z}}^k \triangleq \mathbf{x}^T \hat{\mathbf{w}}^k$ , respectively. The corresponding test-error rate<sup>3</sup>  $\mathcal{E}^k \triangleq \Pr\{y \neq \text{sgn}(\hat{\mathbf{z}}^k)\}$  can be computed as follows. Letting  $I_{\{\cdot\}}$  denote an indicator function that assumes the value 1 when its Boolean argument is true and the value 0 otherwise, we have

$$\mathcal{E}^k = \mathbb{E}\{I_{\{y \neq \text{sgn}(\hat{\mathbf{z}}^k)\}}\} \quad (18)$$

$$= \sum_{y \in \{-1, 1\}} \int I_{\{y \neq \text{sgn}(\hat{\mathbf{z}}^k)\}} \int p_{y, \hat{\mathbf{z}}^k, \mathbf{z}}(y, \hat{\mathbf{z}}^k, \mathbf{z}) dz d\hat{\mathbf{z}}^k \quad (19)$$

$$= \sum_{y \in \{-1, 1\}} \iint I_{\{y \neq \text{sgn}(\hat{\mathbf{z}}^k)\}} p_{y|z}(y|z) p_{z, \hat{\mathbf{z}}^k}(z, \hat{\mathbf{z}}^k) dz d\hat{\mathbf{z}}^k. \quad (20)$$

<sup>3</sup>For simplicity we assume a decision rule of the form  $\hat{y}^k = \text{sgn}(\hat{\mathbf{z}}^k)$ , although other decision rules can be accommodated in our analysis.

Furthermore, from the definitions of  $(\mathbf{z}, \hat{\mathbf{z}}^k)$  and the bivariate central limit theorem, we have that

$$\begin{bmatrix} \mathbf{z} \\ \hat{\mathbf{z}}^k \end{bmatrix} \xrightarrow{d} \mathcal{N}(\mathbf{0}, \Sigma_z^k) = \mathcal{N}\left(\begin{bmatrix} 0 \\ 0 \end{bmatrix}, \begin{bmatrix} \Sigma_{11}^k & \Sigma_{12}^k \\ \Sigma_{21}^k & \Sigma_{22}^k \end{bmatrix}\right), \quad (21)$$

where  $\xrightarrow{d}$  indicates convergence in distribution. In [30], it is shown that the above matrix components are

$$\Sigma_{11}^k = \delta^{-1}(\text{var}\{\mathbf{w}_n\} + \mathbb{E}[\mathbf{w}_n]^2), \quad (22)$$

$$\Sigma_{12}^k = \Sigma_{21}^k = \delta^{-1}(\text{cov}\{\mathbf{w}_n, \hat{\mathbf{w}}_n^k\} + \mathbb{E}[\mathbf{w}_n]\mathbb{E}[\hat{\mathbf{w}}_n^k]), \quad (23)$$

$$\Sigma_{22}^k = \delta^{-1}(\text{var}\{\hat{\mathbf{w}}_n^k\} + \mathbb{E}[\hat{\mathbf{w}}_n^k]^2) \quad (24)$$

for label-to-feature ratio  $\delta$ . As described earlier, the above moments can be computed using [18, Algorithm 3]. The integral in (20) can then be computed (numerically if needed) for a given activation function  $p_{y|z}$ , yielding an estimate of GAMP's test-error rate at the  $k^{th}$  iteration.

To validate the accuracy of the above asymptotic analysis, we conducted a Monte-Carlo experiment with data synthetically generated in accordance with the assumed model. In particular, for each of 1000 problem realizations, a true weight vector  $\mathbf{w} \in \mathbb{R}^N$  was drawn i.i.d zero-mean Bernoulli-Gaussian and a feature matrix  $\mathbf{X}$  was drawn i.i.d Gaussian, yielding true scores  $\mathbf{z} = \mathbf{X}\mathbf{w}$ , from which the true labels  $\mathbf{y}$  were randomly drawn using a probit activation function  $p_{y|z}$ . A GAMP weight-vector estimate  $\hat{\mathbf{w}}^\infty$  was then computed using the training data  $(\mathbf{y}_{1:M}, \mathbf{X}_{1:M})$ , from which the test-label estimates  $\{\hat{y}_t^\infty\}_{t=M+1}^{M+T}$  with  $\hat{y}_t^\infty = \text{sgn}(\mathbf{x}_t^T \hat{\mathbf{w}}^\infty)$  were computed and compared to the true test-labels in order to calculate the test-error rate for that realization. Figure 2a plots the Monte-Carlo averaged empirical test-error rates (dashed) and state-evolution predicted rates (solid) as level curves over different combinations of training ratio  $\frac{M}{N}$  and discriminative-feature ratio  $\frac{K}{N}$ , where  $K = \|\mathbf{w}\|_0$  and  $N = 1024$ . Similarly, Fig. 2b plots average empirical MSE versus state-evolution predicted MSE, where  $\text{MSE} = \frac{1}{N} \mathbb{E}\{\|\hat{\mathbf{w}}^\infty - \mathbf{w}\|_2^2\}$ .

In both Fig. 2a and Fig. 2b, the training-to-feature ratio  $\frac{M}{N}$  increases from left to right, and the discriminative-feature ratio  $\frac{K}{N}$  increases from bottom to top. The region to the upper-left of the dash-dotted black line contains ill-posed problems (where the number of discriminative features  $K$  exceeds the number of training samples  $M$ ) for which data was not collected. The remainders of Fig. 2a and Fig. 2b show very close agreement between empirical averages and state-evolution predictions.

## IV. GAMP NONLINEAR STEPS

Section II gave a high-level description of how the GAMP iterations in Algorithm 1 can be applied to binary linear classification and feature selection. In this section, we detail the nonlinear steps used to compute  $(\hat{z}, \tau_z)$  and  $(\hat{x}, \tau_x)$  in lines 5–6, 8–9, 16–17, and 19–20 of Algorithm 1. For sum-product GAMP, we recall that the mean and variance computations in lines 5–6 and 16–17 are computed based on the pdfs in (9) and (10), respectively, and for max-sum GAMP the prox steps in 8–9 are computed using equations (14)–(15) and those in 19–20 are computed similarly.

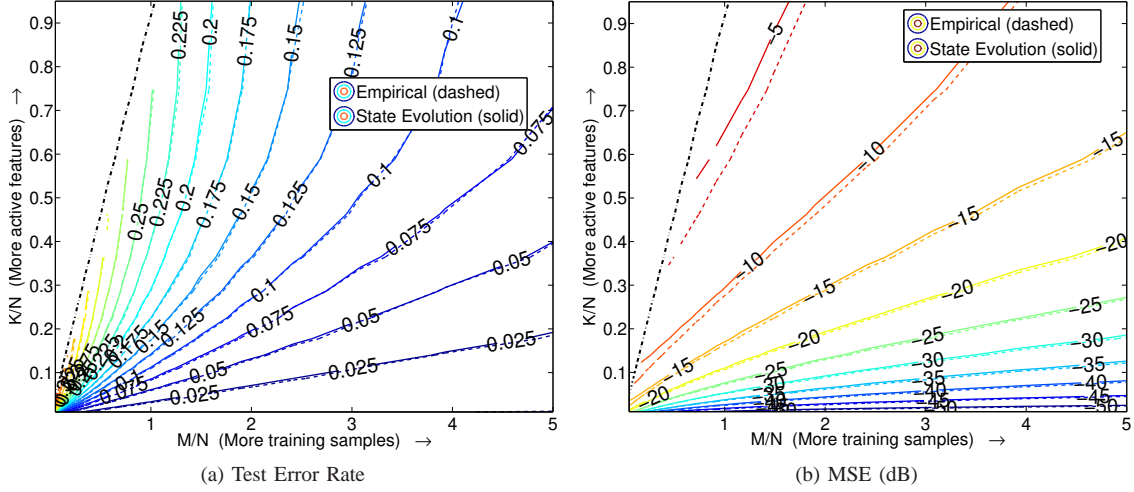


Fig. 2: Test-error rate (a) and mean-squared error (b), versus training-to-feature ratio  $M/N$  and discriminative-feature ratio  $K/N$ , calculated using empirical averaging (dashed) and state-evolution prediction (solid), assuming i.i.d Bernoulli-Gaussian weight vectors and a probit activation function.

### A. Logistic Activation Function

Arguably the most popular activation function for binary linear classification is the logistic sigmoid [1, §4.3.2], [31]:

$$p_{y|z}(y|z; \alpha) = \frac{1}{1 + \exp(-y\alpha z)}, \quad y \in \{-1, 1\} \quad (25)$$

where  $\alpha > 0$  controls the steepness of the transition.

For logistic sum-product GAMP, we propose to compute the mean and variance  $(\hat{z}, \tau_z)$  of the marginal posterior approximation (9) using the variational approach in Algorithm 2, whose derivation is relegated to [30] for reasons of space. We note that Algorithm 2 is reminiscent of the one presented in [1, §10.6], but is more general in that it handles  $\alpha \neq 1$ .

For logistic max-sum GAMP,  $\hat{z}$  from (14) solves the scalar minimization problem (16) with  $f(u) = -\log p_{y|z}(y|u; \alpha)$  from (25), which is convex. To find this  $\hat{z}$ , we use bisection search to locate the root of  $\frac{d}{du}[f(u) + \frac{1}{2\tau} (u - v)^2]$ . The max-sum  $\tau_z$  from (15) can then be computed in closed form using  $\hat{z}$  and  $f''(\cdot)$  via (17). Note that, unlike the classical ML-based approach to logistic regression (e.g., [1, §4.3.3]), GAMP performs only scalar minimizations and thus does not need to construct or invert a Hessian matrix.

---

### Algorithm 2 A Variational Approach to Logistic Activation Functions for Sum-Product GAMP

---

**Input:** Class label  $y \in \{-1, 1\}$ , logistic scale  $\alpha$ , and GAMP-computed parameters  $\hat{p}$  and  $\tau_p$  (see (9))

**Initialize:**  $\xi \leftarrow \sqrt{\tau_p + |\hat{p}|^2}$

```

1: repeat
2:    $\sigma \leftarrow (1 + \exp(-\alpha\xi))^{-1}$ 
3:    $\lambda \leftarrow \frac{\alpha}{2\xi}(\sigma - \frac{1}{2})$ 
4:    $\tau_z \leftarrow \tau_p(1 + 2\tau_p\lambda)^{-1}$ 
5:    $\hat{z} \leftarrow \tau_z(\hat{p}/\tau_p + \alpha y/2)$ 
6:    $\xi \leftarrow \sqrt{\tau_z + |\hat{z}|^2}$ 
7: until Terminated
8: return  $\hat{z}, \tau_z$ 

```

---

Quantity	Value
$c$	$\frac{\hat{p}}{\sqrt{v + \tau_p}}$
$\hat{z}$	$\hat{p} + \frac{y\tau_p\phi(c)}{\Phi(yc)\sqrt{v + \tau_p}}$
$\tau_z$	$\tau_p - \frac{\tau_p^2\phi(c)}{\Phi(yc)(v + \tau_p)} \left( yc + \frac{\phi(c)}{\Phi(c)} \right)$

TABLE I: Sum-product GAMP computations for probit activation function.

### B. Probit Activation Function

Another popular activation function is the probit [1, §4.3.5]:

$$p_{y|z}(1|z; v) = \int_{-\infty}^z \mathcal{N}(\tau; 0, v) d\tau = \Phi\left(\frac{z}{\sqrt{v}}\right) \quad (26)$$

where  $p_{y|z}(-1|z) = 1 - p_{y|z}(1|z) = \Phi(-\frac{z}{\sqrt{v}})$  and where  $v > 0$  controls the steepness of the sigmoid.

Unlike the logistic case, the probit case leads to closed-form sum-product GAMP computations. In particular, the density (9) corresponds to the posterior pdf of a random variable  $z$  with prior  $\mathcal{N}(\hat{p}, \tau_p)$  from an observation  $y = y$  measured under the likelihood model (26). A derivation in [32, §3.9] provides the necessary expressions for these moments when  $y = 1$ , and a similar exercise tackles the  $y = -1$  case. For completeness, the sum-product computations are summarized in Table I. Max-sum GAMP computation of  $(\hat{z}, \tau_z)$  can be performed using a bisection search akin to that described in Section IV-A.

### C. Hinge-Loss Activation Function

The *hinge loss*  $f_{z_m}(z) \triangleq \max(0, 1 - y_m z)$  is commonly used in the *support vector machine* (SVM) approach to maximum-margin classification [1, §7.1], i.e.,

$$\hat{\mathbf{w}} = \arg \min_{\mathbf{w}} \sum_{m=1}^M f_{z_m}(\mathbf{x}_m^\top \mathbf{w}) + \lambda \|\mathbf{w}\|_2^2 \quad (27)$$

or variations where  $\|\mathbf{w}\|_2^2$  is replaced with a sparsity-inducing alternative like  $\|\mathbf{w}\|_1$  [33]. Recalling Section II-B, this loss

Quantity	Value
$\hat{z}$	$(1 + \gamma_y)^{-1} \underline{\mu}_y + (1 + \gamma_y^{-1})^{-1} \bar{\mu}_y$
$\tau_z$	$(1 + \gamma_y)^{-1} (\underline{v}_y + \underline{\mu}_y^2) + (1 + \gamma_y^{-1})^{-1} (\bar{v}_y + \bar{\mu}_y^2) - \hat{z}^2$

TABLE II: Sum-product GAMP computations for the hinge-loss activation function. See Appendix A for definitions of  $\gamma_y$ ,  $\underline{\mu}_y$ ,  $\bar{\mu}_y$ ,  $\underline{v}_y$ ,  $\bar{v}_y$ .

Quantity	Value
$C_y$	$\frac{\gamma}{\gamma + (1 - 2\gamma)C_y^*}$
$\hat{z}$	$C_y \hat{p} + (1 - C_y) \hat{z}^*$
$\tau_z$	$C_y (\tau_p + \hat{p}^2) + (1 - C_y) (\tau_z^* + (\hat{z}^*)^2) - \hat{z}^2$

TABLE III: Sum-product GAMP computations for a robustified activation function. See text for definitions of  $C_y^*$ ,  $\hat{z}^*$ , and  $\tau_z^*$ .

leads to the activation function

$$p_{y_m|z_m}(y_m|z) \propto \exp(-\max(0, 1 - y_m z)). \quad (28)$$

For hinge-loss sum-product GAMP, the mean and variance  $(\hat{z}, \tau_z)$  of (9) can be computed in closed form using the procedure described in Appendix A, and summarized in Table II. Meanwhile, for max-sum GAMP, the proximal steps (14)-(15) can be efficiently computed using bisection search, as in the logistic and probit cases.

#### D. A Method to Robustify Activation Functions

In some applications, a fraction  $\gamma \in (0, 1)$  of the training labels are known<sup>4</sup> to be corrupted, or at least highly atypical under a given activation model  $p_{y|z}^*(y|z)$ . As a robust alternative to  $p_{y|z}^*(y|z)$ , Opper and Winther [34] proposed to use

$$p_{y|z}(y|z; \gamma) = (1 - \gamma) p_{y|z}^*(y|z) + \gamma p_{y|z}^*(-y|z) \quad (29)$$

$$= \gamma + (1 - 2\gamma) p_{y|z}^*(y|z). \quad (30)$$

We now describe how the GAMP nonlinear steps for an arbitrary  $p_{y|z}^*$  can be used to compute the GAMP nonlinear steps for a robust  $p_{y|z}$  of the form in (30).

In the sum-product case, knowledge of the non-robust quantities  $\hat{z}^* \triangleq \frac{1}{C_y^*} \int_z z p_{y|z}^*(y|z) \mathcal{N}(z; \hat{p}, \tau_p)$ ,  $\tau_z^* \triangleq \frac{1}{C_y^*} \int_z (z - \hat{z}^*)^2 p_{y|z}^*(y|z) \mathcal{N}(z; \hat{p}, \tau_p)$ , and  $C_y^* \triangleq \int_z p_{y|z}^*(y|z) \mathcal{N}(z; \hat{p}, \tau_p)$  is sufficient for computing the robust sum-product quantities  $(\hat{z}, \tau_z)$ , as summarized in Table III. (See [30] for details.)

In the max-sum case, computing  $\hat{z}$  in (14) involves solving the scalar minimization problem in (16) with  $f(u) = -\log p_{y|z}(y|u; \gamma) = -\log[\gamma + (1 - 2\gamma) p_{y|z}^*(y|u)]$ . As before, we use a bisection search to find  $\hat{z}$  and then we use  $f''(\hat{z})$  to compute  $\tau_z$  via (17).

#### E. Weight Vector Priors

We now discuss the nonlinear steps used to compute  $(\hat{w}, \tau_w)$ , i.e., lines 16-17 and 19-20 of Algorithm 1. These steps are, in fact, identical to those used to compute  $(\hat{z}, \tau_z)$

<sup>4</sup>A method to learn an unknown  $\gamma$  will be proposed in Section V.

Quantity	Value
SPG	$\hat{w} = (C\underline{\mu} + \bar{C}\bar{\mu}) / (C + \bar{C})$ $\tau_w = (C(\underline{v} + \underline{\mu}^2) + \bar{C}(\bar{v} + \bar{\mu}^2)) / (C + \bar{C}) - \hat{w}^2$
MSG	$\hat{w} = \text{sgn}(\sigma \hat{r}) \max( \sigma \hat{r}  - \lambda_1 \sigma^2, 0)$ $\tau_w = \sigma^2 \cdot \mathbf{I}_{\{\hat{w} \neq 0\}}$

TABLE IV: Sum-product GAMP (SPG) and max-sum GAMP (MSG) computations for the elastic-net regularizer  $f_{\mathbf{w}_n}(w) = \lambda_1|w| + \lambda_2 w^2$ , which includes  $\ell_1$  or Laplacian-prior (via  $\lambda_2 = 0$ ) and  $\ell_2$  or Gaussian-prior (via  $\lambda_1 = 0$ ) as special cases. See Table V for definitions of  $\underline{C}$ ,  $\bar{C}$ ,  $\underline{\mu}$ ,  $\bar{\mu}$ , etc.

except that the prior  $p_{\mathbf{w}_n}(\cdot)$  is used in place of the activation function  $p_{y_m|z_m}(y_m|\cdot)$ . For linear classification and feature selection in the  $N \gg M$  regime, it is customary to choose a prior  $p_{\mathbf{w}_n}(\cdot)$  that leads to sparse (or approximately sparse) weight vectors  $\mathbf{w}$ , as discussed below.

For sum-product GAMP, this can be accomplished by choosing a Bernoulli- $\tilde{p}$  prior, i.e.,

$$p_{\mathbf{w}_n}(w) = (1 - \pi_n) \delta(w) + \pi_n \tilde{p}_{\mathbf{w}_n}(w), \quad (31)$$

where  $\delta(\cdot)$  is the Dirac delta function,  $\pi_n \in [0, 1]$  is the prior<sup>5</sup> probability that  $\mathbf{w}_n = 0$ , and  $\tilde{p}_{\mathbf{w}_n}(\cdot)$  is the pdf of a non-zero  $\mathbf{w}_n$ . While Bernoulli-Gaussian [35] and Bernoulli-Gaussian-mixture [23] are common choices, Section VII suggests that Bernoulli-Laplacian also performs well.

In the max-sum case, the GAMP nonlinear outputs  $(\hat{w}, \tau_w)$  are computed via

$$\hat{w} = \text{prox}_{\tau_r f_{\mathbf{w}_n}}(\hat{r}) \quad (32)$$

$$\tau_w = \tau_r \text{prox}'_{\tau_r f_{\mathbf{w}_n}}(\hat{r}) \quad (33)$$

for a suitably chosen regularizer  $f_{\mathbf{w}_n}(w)$ . Common examples include  $f_{\mathbf{w}_n}(w) = \lambda_1|w|$  for  $\ell_1$  regularization [19],  $f_{\mathbf{w}_n}(w) = \lambda_2 w^2$  for  $\ell_2$  regularization [18], and  $f_{\mathbf{w}_n}(w) = \lambda_1|w| + \lambda_2 w^2$  for the “elastic net” [36]. As described in Section II-B, any regularizer  $f_{\mathbf{w}_n}$  can be interpreted as a (possibly improper) prior pdf  $p_{\mathbf{w}_n}(w) \propto \exp(-f_{\mathbf{w}_n}(w))$ . Thus,  $\ell_1$  regularization corresponds to a Laplacian prior,  $\ell_2$  to a Gaussian prior, and the elastic net to a product of Laplacian and Gaussian pdfs.

In Table VII, we give the sum-product and max-sum computations for the prior corresponding to the elastic net, which includes both Laplacian (i.e.,  $\ell_1$ ) and Gaussian (i.e.,  $\ell_2$ ) as special cases; a full derivation can be found in [30]. For the Bernoulli-Laplacian case, these results can be combined with the Bernoulli- $\tilde{p}$  extension in Table VII.

#### F. The GAMPmatlab Software Suite

The GAMP iterations from Algorithm 1, including the nonlinear steps discussed in this section, have been implemented in the open-source “GAMPmatlab” software suite.<sup>6</sup> For convenience, the existing activation-function implementations are summarized in Table VI and relevant weight-prior implementations appear in Table VII.

<sup>5</sup>In Section V we describe how a common  $\pi = \pi_n \forall n$  can be learned and in Section VI we describe how  $\{\pi_n\}$  can be learned.

<sup>6</sup>The latest source code can be obtained through the GAMPmatlab SourceForge Subversion repository at <http://sourceforge.net/projects/gampmatlab/>.

$\sigma \triangleq \sqrt{\tau_r/(2\lambda_2\tau_r + 1)}$	$\ddot{r} \triangleq \hat{r}/(\sigma(2\lambda_2\tau_r + 1))$
$\underline{r} \triangleq \ddot{r} + \lambda_1\sigma$	$\bar{r} \triangleq \ddot{r} - \lambda_1\sigma$
$C \triangleq \frac{\lambda_1}{2} \exp\left(\frac{\underline{r}^2 - \ddot{r}^2}{2}\right) \Phi(-\underline{r})$	$\bar{C} \triangleq \frac{\lambda_1}{2} \exp\left(\frac{\bar{r}^2 - \ddot{r}^2}{2}\right) \Phi(\bar{r})$
$\underline{\mu} \triangleq \sigma\underline{r} - \sigma\phi(-\underline{r})/\Phi(-\underline{r})$	$\bar{\mu} \triangleq \sigma\bar{r} + \sigma\phi(\bar{r})/\Phi(\bar{r})$
$v \triangleq \sigma^2 \left[ 1 - \frac{\phi(\underline{r})}{\Phi(\underline{r})} \left( \frac{\phi(\underline{r})}{\Phi(\underline{r})} - \underline{r} \right) \right]$	$\bar{v} \triangleq \sigma^2 \left[ 1 - \frac{\phi(\bar{r})}{\Phi(\bar{r})} \left( \frac{\phi(\bar{r})}{\Phi(\bar{r})} + \bar{r} \right) \right]$

TABLE V: Definitions of elastic-net quantities used in Table IV.

Name	$p_{y z}(y z)$	Description	Sum-Product	Max-Sum
Logistic	$\propto (1 + \exp(-\alpha y z))^{-1}$	VI	RF	
Probit	$\Phi\left(\frac{yz}{v}\right)$	CF	RF	
Hinge Loss	$\propto \exp(-\max(0, 1 - yz))$	CF	RF	
Robust- $p^*$	$\gamma + (1 - 2\gamma)p_{y z}^*(y z)$	CF	RF	

TABLE VI: Activity-functions and their GAMPmatlab sum-product and max-sum implementation method: CF = closed form, VI = variational inference, RF = root-finding.

## V. ONLINE PARAMETER TUNING

The activation functions and weight-vector priors described in Section IV depend on modeling parameters that, in practice, must be tuned. For example, the logistic sigmoid (25) depends on  $\alpha$ ; the probit depends on  $v$ ;  $\ell_1$  regularization depends on  $\lambda$ ; and the Bernoulli-Gaussian-mixture prior depends on  $\pi$  and  $\{\omega_l, \mu_l, \sigma_l^2\}_{l=1}^L$ , where  $\omega_l$  parameterizes the weight,  $\mu_l$  the mean, and  $\sigma_l^2$  the variance of the  $l$ th mixture component. Although cross-validation (CV) is the customary approach to tuning parameters such as these, it suffers from two major drawbacks: First, it can be very computationally costly, since each parameter must be tested over a grid of hypothesized values and over multiple data folds. For example,  $K$ -fold cross-validation tuning of  $P$  parameters using  $G$  hypothesized values of each requires the design and evaluation of  $KG^P$  classifiers. Second, leaving out a portion of the training data for CV can degrade classification performance, especially in the example-starved regime where  $M \ll N$  (see, e.g., [37]).

As an alternative to CV, we consider *online learning* of the unknown model parameters  $\theta$  using the methodology from [23], [38]. Here, the goal is to compute the maximum-likelihood estimate  $\hat{\theta}_{\text{ML}} = \arg \max_{\theta} p_{\mathbf{y}}(\mathbf{y}; \theta)$ , where our data model implies a likelihood function of the form

$$p_{\mathbf{y}}(\mathbf{y}; \theta) = \int_{\mathbf{w}} \prod_m p_{y_m|z_m}(y_m | \mathbf{x}^\top \mathbf{w}; \theta) \prod_n p_{w_n}(w_n; \theta). \quad (34)$$

Because it is computationally infeasible to evaluate and/or maximize (34) directly, approximate-ML estimation is performed using expectation-maximization (EM) [39], treating  $\mathbf{w}$  as the “hidden” data, which yields the iteration- $j$  estimate

$$\theta^j = \arg \max_{\theta} \mathbb{E}_{\mathbf{w}|\mathbf{y}} \{ \log p_{\mathbf{y}, \mathbf{w}}(\mathbf{y}, \mathbf{w}; \theta) | \mathbf{y}; \theta^{j-1} \} \quad (35)$$

$$\begin{aligned} &= \arg \max_{\theta} \sum_m \mathbb{E}_{z_m|\mathbf{y}} \{ \log p_{y_m|z_m}(y_m | z_m; \theta) | \mathbf{y}; \theta^{j-1} \} \\ &\quad + \sum_m \mathbb{E}_{\mathbf{w}_n|\mathbf{y}} \{ \log p_{w_n}(w_n; \theta) | \mathbf{y}; \theta^{j-1} \}. \end{aligned} \quad (36)$$

Name	$p_{\mathbf{w}_n}(w)$	Description	Sum-Product	Max-Sum
Gaussian	$\mathcal{N}(w; \mu, \sigma^2)$	CF	CF	
GM	$\sum_l \omega_l \mathcal{N}(w; \mu_l, \sigma_l^2)$	CF	NI	
Laplacian	$\propto \exp(-\lambda w )$	CF	CF	
Elastic Net	$\propto \exp(-\lambda_1 w  - \lambda_2 w^2)$	CF	CF	
Bernoulli- $\tilde{p}$	$(1 - \pi_n)\delta(w) + \pi_n \tilde{p}_{\mathbf{w}_n}(w)$	CF	NA	

TABLE VII: Weight-coefficient priors and their GAMPmatlab sum-product and max-sum implementation method: CF = closed form, NI = not implemented, NA = not applicable.

Furthermore, to evaluate the conditional expectations in (36), GAMP’s posterior approximations from (9)-(10) are used. It was shown in [40] that, in the large-system limit, the estimates generated by this procedure are asymptotically consistent (as  $j \rightarrow \infty$  and under certain identifiability conditions). Moreover, it was shown in [23], [38] that, for various priors and likelihoods of interest in compressive sensing (e.g., AWGN likelihood, Bernoulli-Gaussian-Mixture priors,  $\ell_1$  regularization), the quantities needed from the expectation in (36) are implicitly computed by GAMP, making this approach computationally attractive. However, because this EM procedure runs GAMP several times, once for each EM iteration (although not necessarily to convergence), the total runtime may be increased beyond that of GAMP without EM.

In this work, we export the EM-GAMP methods from [23], [38] to the classification setting, which requires deriving the EM updates for the activation-function parameters, such as  $\alpha$  in the logistic model (25),  $v$  in the probit model (26), and  $\gamma$  in the robust model (30). (See [30] for details.) To learn  $\gamma$ , it helps to also include the label corruption indicators  $\beta \in \{0, 1\}^M$  in the EM-algorithm’s hidden data (where  $\beta_m = 0$  indicates that  $y_m$  was corrupt, and  $\beta_m = 1$  that it was not), where an i.i.d assumption on the corruption mechanism implies the prior  $p(\beta; \gamma) = \prod_{m=1}^M \gamma^{1-\beta_m} (1 - \gamma)^{\beta_m}$ . In this case, it can be shown [30] that the update of the  $\gamma$  parameter reduces to

$$\gamma^{j+1} = \arg \max_{\gamma \in [0, 1]} \sum_{m=1}^M \mathbb{E}_{\beta_m|\mathbf{y}} [\log p(\beta_m; \gamma) | \mathbf{y}; \theta^j] \quad (37)$$

$$= \frac{1}{M} \sum_{m=1}^M p(\beta_m = 0 | \mathbf{y}; \theta^j), \quad (38)$$

where (38) leveraged  $\mathbb{E}[\beta_m|\mathbf{y}; \theta^j] = 1 - p(\beta_m = 0 | \mathbf{y}; \theta^j)$ . Moreover,  $p(\beta_m = 0 | \mathbf{y}; \theta^j)$  is easily computed using quantities returned by sum-product GAMP.

## VI. STRUCTURED SPARSITY AND TURBO FEATURE SELECTION

The GAMP algorithm proposed in [18] and summarized in Section II is premised on statistically independent weights  $\{\mathbf{w}_n\}$ , so that the weight-vector prior  $p_{\mathbf{w}}$  decouples as in (8). In some classification or feature-selection problems, however, classification accuracy and/or interpretability are improved by modeling the weights in  $\mathbf{w}$  as statistically dependent. We now describe how the “turbo” extension of sum-product GAMP,

proposed in [35] and generalized in [22], can be used to tackle the case of statistically dependent weights.

As a concrete starting point, we first consider a *structured sparsity* model that, in addition to promoting sparsity in  $\mathbf{w}$ , promotes “clustering” among the non-zero-coefficient locations in the following sense: if  $\mathbf{w}_n \neq 0$  then it is probable that  $\mathbf{w}_j \neq 0$  for indices  $j$  in some neighborhood of  $n$ , while if  $\mathbf{w}_n = 0$  then it is probable that  $\mathbf{w}_j = 0$  for indices  $j$  in some neighborhood of  $n$ . In other words, if the  $n$ th feature is discriminative, then features in a neighborhood of  $n$  tend to also be discriminative, and vice versa. (See Section VII-C for a motivating application from cognitive neuroscience.) Using the (hidden) “support” variable  $\mathbf{s}_n \in \{-1, 1\}$  to indicate whether  $\mathbf{w}_n \neq 0$  (using  $\mathbf{s}_n = 1$ ) or  $\mathbf{w}_n = 0$  (using  $\mathbf{s}_n = -1$ ), the resulting weight-vector prior can be expressed as

$$p_{\mathbf{w}}(\mathbf{w}) = \sum_{\mathbf{s} \in \{-1, 1\}^N} p_{\mathbf{s}}(\mathbf{s}) p_{\mathbf{w}|\mathbf{s}}(\mathbf{w}|\mathbf{s}) \quad (39)$$

$$= \sum_{\mathbf{s} \in \{-1, 1\}^N} p_{\mathbf{s}}(\mathbf{s}) \prod_{n=1}^N p_{\mathbf{w}_n|\mathbf{s}_n}(\mathbf{w}_n|\mathbf{s}_n), \quad (40)$$

where in (40) we assumed (for simplicity) that the weights are *conditionally* independent; see [22] for more sophisticated models. Since we are focusing on the sum-product case, the Bernoulli- $\tilde{p}$  model (31) implies that

$$p_{\mathbf{w}_n|\mathbf{s}_n}(\mathbf{w}_n|\mathbf{s}_n) = \begin{cases} \delta(\mathbf{w}_n) & \mathbf{s}_n = -1 \\ \tilde{p}_{\mathbf{w}_n}(\mathbf{w}_n) & \mathbf{s}_n = 1 \end{cases} \quad (41)$$

for suitably chosen active-weight pdf  $\tilde{p}_{\mathbf{w}_n}$  (e.g., Gaussian, GM, or Laplacian). Finally, we model the support vector  $\mathbf{s}$  as a Markov Random Field (MRF) using [41, §2.1]

$$p_{\mathbf{s}}(\mathbf{s}) \propto \exp \left( \beta \sum_n \sum_{j \in \mathcal{V}_n} s_n s_j - \alpha \sum_n s_n \right), \quad (42)$$

where  $\beta$  controls the amount of clustering,  $\alpha$  (partially) governs the sparsity rate, and  $\mathcal{V}_n$  is the neighborhood of  $n$ .

The resulting joint pdf  $p_{\mathbf{y}, \mathbf{w}, \mathbf{s}}(\mathbf{y}, \mathbf{w}, \mathbf{s})$  factorizes in the manner illustrated by Fig. 3. To perform inference on this model, we partition the factor graph into the two subgraphs shown in Fig. 3, noting that the left subgraph has the same structure as Fig. 1b and thus allows the application of GAMP, while the right subgraph has an MRF structure and thus can be handled by standard techniques [42]. The “turbo” approach [35], inspired by turbo-decoding methods in modern communication receivers [26], merges the two subgraphs using the sum-product algorithm, which repeatedly passes extrinsic support probabilities back and forth between the subgraphs until they converge. A related approach to the exploitation of MRF-based structured sparsity in the context of compressive sensing was proposed in [43].

In summary, the turbo inference procedure described above extends the GAMP framework to facilitate the use of weight-vector models with dependent elements  $\mathbf{w}$  in the GAMP framework. Moreover, the EM parameter learning process described in Section V can be used to learn the MRF parameters  $\alpha$  and  $\beta$  in (42) online, eliminating the need for multi-

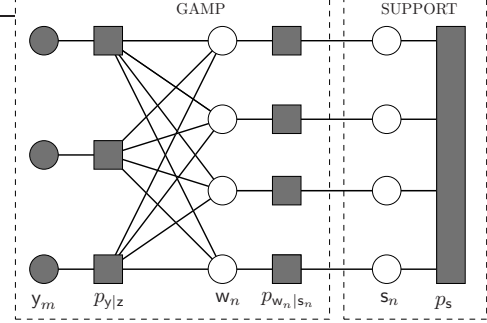


Fig. 3: Factor graph representation of  $p_{\mathbf{y}, \mathbf{w}, \mathbf{s}}$ , with white/grey circles denoting unobserved/observed random variables, and rectangles denoting pdf “factors”.

parameter cross-validation.<sup>7</sup> In Section VII-C we investigate the performance of this MRF structured sparsity model on a popular fMRI classification dataset.

## VII. NUMERICAL STUDY

In this section we describe several real and synthetic classification problems to which GAMP was applied. Our goal throughout the study was primarily to explore those aspects of GAMP which make it unique, including the EM-based parameter tuning described in Section V, and the turbo feature selection procedure of Section VI. Experiments were conducted on a workstation running Red Hat Enterprise Linux (r2.4), with an Intel Core i7-2600 CPU (3.4 GHz, 8MB cache) and 8GB DDR3 RAM.

### A. Text Classification and Adaptive Learning

We first consider a binary text classification problem based on the Reuter’s Corpus Volume I (RCV1) dataset [45]. As in [17], [46], newswire article topic codes CCAT and ECAT were combined to form the positive class while GCAT and MCAT were combined to form constitute the negative class.<sup>8</sup> Although the original dataset consisted of 20 242 balanced training examples of  $N = 47\,236$  features, with 677 399 examples reserved for testing, we followed the approach in [17], [46] and swapped training and testing sets in order to test computational efficiency on a large training dataset (and thus  $M = 677\,399$ ). As in [17], we constructed feature vectors as cosine-normalized logarithmic transformations of the TF-IDF (term frequency-inverse document frequency) data vectors. We note that the resulting features are very sparse; only 0.16% of the entries in  $\mathbf{X}$  are non-zero. Finally, we trained linear classifiers (i.e., weight vectors) using four GAMP-based methods and three existing state-of-the-art methods: TFOCS [47] in L1-LR mode, CDN [17], and TRON [48]. In doing so, for EM learning we used 5 EM iterations, and for cross-validation we used 2 folds and a logarithmically spaced grid size of 10.

<sup>7</sup>Further details on the mean-field EM approach [44] used to learn the MRF parameters can be found in [30].

<sup>8</sup>Data was taken from <http://www.csie.ntu.edu.tw/~cjlin/libsvmtools/datasets/binary.html>.

Classifier	Tuning	Accuracy	Runtime (s)	Density
spGAMP: BG-PR	EM	97.6%	<b>317 / 57</b>	11.1%
spGAMP: BG-HL	EM	<b>97.7%</b>	468 / 93	<b>8.0%</b>
msGAMP: L1-LR	EM	97.6%	684 / 123	9.8%
msGAMP: L1-LR	xval	97.6%	3068 / 278	19.6%
CDN	xval	<b>97.7%</b>	1298 / 112	10.9%
TRON	xval	<b>97.7%</b>	1682 / 133	10.8%
TFOCS: L1-LR	xval	97.6%	1086 / 94	19.2%

TABLE VIII: A comparison of different classifiers on the RCV1 binary dataset (with training/testing sets flipped), showing the test-set classification accuracy, the total and post-tuning runtimes, and the density of the weight vector. Above, sp = sum-product; ms = max-sum; BG = Bernoulli-Gaussian; PR = Probit; HL = Hinge loss; L1 =  $\ell_1$  regularization; LR = Logistic.

Table VIII summarizes the performance achieved by the resulting classifiers, including the test-set classification accuracy, weight-vector density (i.e., the fraction of non-zero weights),<sup>9</sup> and two runtimes: the *total* runtime needed to train the classifier, which includes EM- or cross-validation-based parameter tuning, and the *post-tuning* runtime. Although it is customary to report only the latter, we feel that the former better captures the true computational cost of classifier design.

Table VIII shows all 7 classifiers achieving nearly identical test-set classification accuracy. However, if feature selection is the goal, then weight-vector density is also important, and for this we see significant differences among algorithms. Notably, the two most discriminative (i.e., sparse) classifiers are the result of EM-GAMP methods. We attribute this sparsity in large part to EM-tuning, since Table VIII shows that when cross-validation is used in place of EM-tuning with L1-LR GAMP, the weight vector is twice as dense.

Table VIII also shows a wide range of runtimes. Among the post-tuning runtimes, the two fastest are EM-GAMP based. Moreover, among the total runtimes, the three fastest are EM-GAMP based, with the best (at 317 seconds) beating the fastest non-GAMP algorithm (at 1086 seconds) by more than a factor of 3. That said, some caution must be used when comparing runtimes. For example, while all algorithms were given a “stopping tolerance” of  $10^{-3}$ , the algorithms apply this tolerance in different ways. Also, CDN and TRON are implemented in C++, while GAMP is implemented in object-oriented MATLAB (and therefore is far from optimized).

Finally, we note that, although GAMP was derived under the assumption that the elements of  $\mathbf{X}$  are realizations of a an i.i.d sub-Gaussian distribution, it worked well even with the  $\mathbf{X}$  of this experiment, which was far from i.i.d sub-Gaussian. We attribute the robust performance of GAMP to the adaptive damping mechanism included in the GAMPmatlab implementation (described in [49]).

### B. Robust Classification

In Section IV-D, we proposed an approach by which GAMP can be made robust to labels that are corrupted or otherwise highly atypical under a given activation model  $p_{y|z}^*$ . We now

<sup>9</sup>Since the weights returned by sum-product BG-GAMP are non-zero with probability one, the model density is defined as the fraction of posterior support probabilities  $p(w_n \neq 0|y)$  that exceed 1/2.

evaluate the performance of this robustification method. To do so, we first generated examples<sup>10</sup>  $(y_m, \mathbf{x}_m)$  with balanced classes such that the Bayes-optimal classification boundary is a hyperplane with a desired Bayes error rate of  $\varepsilon_B$ . Then, we flipped a fraction  $\gamma$  of the training labels (but not the test labels), trained several different varieties of GAMP classifiers, and measured their classification accuracy on the test data.

The first classifier we considered paired a genie-aided “standard logistic” activation function, (25), with an i.i.d. zero-mean, unit-variance Gaussian weight vector prior. Note that under a class-conditional Gaussian generative distribution with balanced classes, the corresponding activation function is logistic with scale parameter  $\alpha = 2M\mu$  [31]. Therefore, the genie-aided logistic classifier was provided the true value of  $\mu$ , which was used to specify the logistic scale  $\alpha$ . The second classifier we considered paired a genie-aided robust logistic activation function, which possessed perfect knowledge of both  $\mu$  and the mislabeling probability  $\gamma$ , with the aforementioned Gaussian weight vector prior. To understand how performance is impacted by the parameter tuning scheme of Section V, we also trained EM variants of the preceding classifiers. The EM-enabled standard logistic classifier was provided a fixed logistic scale of  $\alpha = 100$ , and was allowed to tune the variance of the weight vector prior. The EM-enabled robust logistic classifier was similarly configured, and in addition was given an initial mislabeling probability of  $\gamma^0 = 0.01$ , which was updated according to (38).

In Fig. 4, we plot the test error rate for each of the four GAMP classifiers as a function of the mislabeling probability  $\gamma$ . For this experiment,  $\mu$  was set so as to yield a Bayes error rate of  $\varepsilon_B = 0.05$ .  $M = 8192$  training examples of  $N = 512$  training features were generated independently, with the test set error rate evaluated based on 1024 unseen (and uncorrupted) examples. Examining the figure, we can see that EM parameter tuning is beneficial for both the standard and robust logistic classifiers, although the benefit is more pronounced for the standard classifier. Remarkably, both the genie-aided and EM-tuned robust logistic classifiers are able to cope with an extreme amount of mislabeling while still achieving the Bayes error rate, thanks in part to the abundance of training data.

### C. fMRI Classification with turboGAMP

As cognitive neuroscientists study how the human brain functions at a physical level, classification algorithms have become an important tool for analyzing functional MRI (fMRI) and scalp electro/magnetoencephalography (EEG/MEG) data [50], [51]. For neuroscientists, the value of a classifier is not in its *ability* to distinguish between a subject’s cognitive states, but rather in the insights gleaned from understanding *how* the classifier does so. By learning what brain regions the classifier believes are important for differentiating the cognitive states,

<sup>10</sup>Data was generated according to a class-conditional Gaussian distribution with  $N$  discriminatory features. Specifically, given the label  $y \in \{-1, 1\}$  a feature vector  $\mathbf{x}$  was generated as follows: entries of  $\mathbf{x}$  were drawn i.i.d  $\mathcal{N}(y\mu, M^{-1})$  for some  $\mu > 0$ . Under this model, with balanced classes, the Bayes error rate can be shown to be  $\varepsilon_B = \Phi(-\sqrt{NM}\mu)$ . The parameter  $\mu$  can then be chosen to achieve a desired  $\varepsilon_B$ .

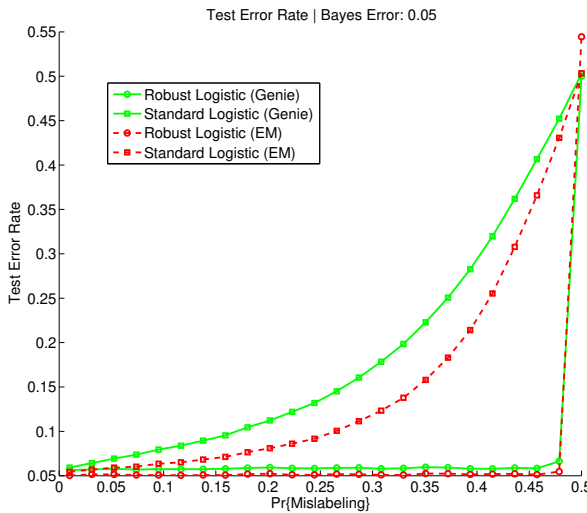


Fig. 4: Test error rate of genie-aided (solid curves) and EM-tuned (dashed curves) instances of standard logistic ( $\square$ ) and robust logistic ( $\circ$ ) classifiers as a function of mislabeling probability  $\gamma$ , with  $M = 8192$ ,  $N = 512$ , and Bayes error rate  $\varepsilon_B = 0.05$ .

neuroscientists hope to gain insight into the underlying neural processes by which the brain operates.

Early techniques for interpreting neuroimaging data relied largely on univariate statistics computed on a voxel-by-voxel basis [50], however, there appears to be growing consensus amongst cognitive neuroscientists that interactions across spatially diverse regions of the cortex play an important role in cognition [3], [50]–[52]. In response, a number of *multi-voxel pattern analysis* (MVPA) techniques have emerged in recent years, employing pattern classification strategies to make better use of the massively multivariate neuroimaging data (e.g., [3]–[5]). While such approaches have yielded positive results, as described by Norman et al. [50], “one of the weaknesses of extant MVPA methods is that the classifier is not provided with information about spatial relationships between the to-be-classified voxels (i.e., which voxels are nearby in 3D space). As such, classifiers have no natural way to leverage the *topography* of cortical representations – the fact that spatially proximate voxels tend to represent similar things.”<sup>11</sup>

To address the aforementioned weakness, using the turboGAMP approach to structured inference described in Section VI, we implemented a 3D MRF-structured classifier that modeled the topographical correlations between voxels, and applied it to the popular Haxby fMRI classification dataset [3]. Our neighborhood set consisted of nearest-neighbor voxels in all directions, i.e., for the  $(i, j, k)^{th}$  interior voxel,  $\mathcal{N}_{i,j,k} \triangleq \{(i-1, j, k), (i+1, j, k), (i, j-1, k), (i, j+1, k), (i, j, k-1), (i, j, k+1)\}$ , with elements removed as-needed at boundary voxels.

The Haxby dataset was collected to study face and object representation in human ventral temporal cortex. It consists of fMRI data collected from 6 subjects, with 12 “runs” per

<sup>11</sup>A notable recent work addressing this weakness is [53], which combines an  $\ell_1$ -penalty on weight vector entries, to encourage sparsity, with a multivariate Gaussian whose covariance matrix encodes the correlational structure of the weights.

Classifier	Accuracy (%)			
	Cat vs. House	Cat vs. Scissors	Face vs. Bottle	Face vs. Shoe
iid-BL PR	98.2	84.7	82.4	94.0
iid-BL LR	<b>99.1</b>	83.3	90.7	93.1
iid-BL HL	98.6	85.6	<b>93.1</b>	<b>95.8</b>
mrf-BL PR	97.2	<b>93.5</b>	92.1	91.7
mrf-BL LR	<b>99.1</b>	80.1	81.5	91.2
mrf-BL HL	78.2	56.0	85.2	88.9

TABLE IX: Test-set accuracy (in %) of sum-product and turbo GAMP classifiers on several pairwise comparisons from the Haxby fMRI dataset (single subject). Above, BL = Bernoulli-Laplace; PR = Probit; HL = Hinge loss; LR = Logistic.

subject. In each run, the subjects passively viewed greyscale images of eight object categories (faces, houses, cats, bottles, scissors, shoes, chairs, and nonsense patterns), grouped in 24s stimulus blocks separated by rest periods. Images were shown for 500ms, with a 1500ms inter-stimulus interval. Full-brain fMRI data were recorded with a volume repetition time of 2.5s, resulting in  $\sim 9$  volumes per stimulus block.

In order to illustrate how an MRF-structured classifier can produce weight vectors that are more interpretable than those produced by conventional, structureless classifiers, we trained various turboGAMP classifiers on data collected from a single subject, estimating the classification error rate by holding out one data run, and training on the remainder (averaging this process across all 12 runs). It is worth re-iterating the objective of MVPA: cognitive neuroscientists are interested in understanding how different regions of the brain work together to accomplish cognitive tasks. Classification algorithms therefore are not useful for their *ability* to distinguish between cognitive states, but rather for the *information* they provide regarding which features are important for discriminating between states. Consequently, the misclassification rate is meaningful only in that it confirms that the classifier is accurately identifying important features; enhancing interpretability, not reducing misclassification rate, is the primary objective.

In Table IX, we summarize the performance of several flavors of i.i.d and 3D MRF turboGAMP classifiers, on different pairwise comparisons (e.g., cat vs. house). In all cases, an EM procedure was used to tune relevant model parameters. As expected, there are comparisons for which the MRF structure does not improve classification accuracy, although an MRF Bernoulli-Laplacian + Probit model does substantially outperform the i.i.d models on the cat vs. scissors comparison.

## VIII. CONCLUSION

In this work, we presented the first comprehensive study of the *generalized approximate message passing* (GAMP) algorithm [18] in the context of linear binary classification. We established that a number of popular discriminative models, including logistic and probit regression, and support vector machines, can be implemented in an efficient manner using the GAMP algorithmic framework, and that GAMP’s state evolution formalism can be used in certain instances to predict

the misclassification rate of these models. In addition, we demonstrated that a number of sparsity-promoting weight vector priors can be paired with these activation functions to encourage feature selection. Importantly, GAMP's message passing framework enables us to learn the hyperparameters that govern our probabilistic models adaptively from the data using expectation-maximization (EM), a trait which can be advantageous when cross-validation proves infeasible. The flexibility imparted by the GAMP framework allowed us to consider several modifications to the basic discriminative models, such as robust classification, which can be effectively implemented using existing non-robust modules. Moreover, by embedding GAMP within a larger probabilistic graphical model, it is possible to consider a wide variety of structured priors on the weight vector, e.g., priors that encourage spatial clustering of important features.

In a numerical study, we confirmed the efficacy of our approach on both real and synthetic classification problems. We found that EM parameter tuning can be both computationally efficient and accurate on a popular text classification problem. We also observed on synthetic data that the robust classification extension can substantially outperform a non-robust counterpart. Finally, drawing inspiration from the field of cognitive neuroscience, we illustrated how structured feature selection can provide enhanced interpretability of fMRI weight vectors in multi-voxel pattern analysis tasks.

## APPENDIX A SUM-PRODUCT GAMP HINGE-LOSS COMPUTATIONS

In this appendix, we describe the steps needed to compute the sum-product GAMP nonlinear steps for the hinge-loss activation function, (28). For convenience, we define the associated *un-normalized* likelihood function

$$\tilde{p}_{y|z}(y|z) \triangleq \exp(-\max(0, 1 - yz)), \quad y \in \{-1, 1\}. \quad (43)$$

Note from (9) that the sum-product  $(\hat{z}, \tau_z)$  can be interpreted as the posterior mean and variance of a random variable,  $z$ , with prior  $\mathcal{N}(\hat{p}, \tau_p)$  and likelihood proportional to  $\tilde{p}_{y|z}(y|z)$ .

To compute the statistics  $\hat{z} \equiv E[z|y = y]$  and  $\tau_z \equiv \text{var}\{z|y = y\}$ , we first write the posterior pdf as

$$p_{z|y}(z|y) = C_y^{-1} \tilde{p}_{y|z}(y|z) p_z(z), \quad (44)$$

where  $C_y$  is an appropriate normalization constant. Defining

$$\alpha_y \triangleq ((1 - \tau_p) - y\hat{p})/\sqrt{\tau_p} \quad (45)$$

$$\beta_y \triangleq (y\hat{p} - 1)/\sqrt{\tau_p} \quad (46)$$

$$\delta_y \triangleq y\hat{p} - 1 + \tau_p/2, \quad (47)$$

it can be shown [30] that

$$C_1 = \int_{-\infty}^1 \exp(z - 1) \mathcal{N}(z; \hat{p}, \tau_p) + \int_1^\infty \mathcal{N}(z; \hat{p}, \tau_p) \quad (48)$$

$$= \exp(\delta_1) \Phi(\alpha_1) + \Phi(\beta_1) \quad (49)$$

The posterior mean for  $y = 1$  is therefore given by

$$E[z|y=1] = \frac{1}{C_1} \int_z z \tilde{p}_{y|z}(y=1|z) p_z(z) \quad (50)$$

$$= \frac{1}{C_1} \left[ e^{\delta_1} \int_{-\infty}^1 z \mathcal{N}(z; \hat{p} + \tau_p, \tau_p) + \int_1^\infty z \mathcal{N}(z; \hat{p}, \tau_p) \right] \quad (51)$$

$$= \frac{e^{\delta_1} \Phi(\alpha_1)}{C_1} \int_{-\infty}^1 z \frac{\mathcal{N}(z; \hat{p} + \tau_p, \tau_p)}{\Phi(\alpha_1)} + \frac{\Phi(\beta_1)}{C_1} \int_1^\infty z \frac{\mathcal{N}(z; \hat{p}, \tau_p)}{\Phi(\beta_1)}, \quad (52)$$

where each integral in (52) represents the first moment of a truncated normal random variable. Similar expressions can be derived for  $E[z|y=-1]$ . Then, defining the quantities

$$\gamma_y \triangleq e^{-\delta_y} \Phi(\beta_y)/\Phi(\alpha_y) \quad (53)$$

$$\mu_y \triangleq \hat{p} + (\tau_p - \sqrt{\tau_p}) \phi(\alpha_y)/\Phi(\alpha_y) \quad (54)$$

$$\bar{\mu}_y \triangleq \hat{p} + y\sqrt{\tau_p} \phi(\beta_y)/\Phi(\beta_y), \quad (55)$$

it can be shown [54] that, for  $y \in \{-1, 1\}$ ,

$$\hat{z}(y) = E[z|y = y] = (1 + \gamma_y)^{-1} \mu_y + (1 + \gamma_y^{-1})^{-1} \bar{\mu}_y. \quad (56)$$

To compute  $\tau_z \equiv \text{var}\{z|y = y\}$ , it suffices to derive an expression for  $E[z^2|y = y]$ . Following the same line of reasoning that produced (52), we find

$$E[z^2|y=1] \quad (57)$$

$$= \frac{e^{\delta_1} \Phi(\alpha_1)}{C_1} \int_{-\infty}^1 z^2 \frac{\mathcal{N}(z; \hat{p} + \tau_p, \tau_p)}{\Phi(\alpha_1)} + \frac{\Phi(\beta_1)}{C_1} \int_1^\infty z^2 \frac{\mathcal{N}(z; \hat{p}, \tau_p)}{\Phi(\beta_1)},$$

where each integral in (57) is the second moment of a truncated normal random variable. A similar expression can be derived for  $E[z^2|y=-1]$ . Defining

$$v_y \triangleq \tau_p \left[ 1 - \frac{\phi(\alpha_y)}{\Phi(\alpha_y)} \left( \frac{\phi(\alpha_y)}{\Phi(\alpha_y)} + \alpha_y \right) \right] \quad (58)$$

$$\bar{v}_y \triangleq \tau_p \left[ 1 - \frac{\phi(\beta_y)}{\Phi(\beta_y)} \left( \frac{\phi(\beta_y)}{\Phi(\beta_y)} + \beta_y \right) \right], \quad (59)$$

it can be shown [54] that

$$E[z^2|y = y] = (1 + \gamma_y)^{-1} (v_y + \mu_y^2) + (1 + \gamma_y^{-1})^{-1} (\bar{v}_y + \bar{\mu}_y^2), \quad (60)$$

allowing us to compute  $\tau_z(y) = E[z^2|y = y] - \hat{z}^2(y)$ .

## REFERENCES

- [1] C. M. Bishop, *Pattern Recognition and Machine Learning*. New York: Springer-Verlag, 2006.
- [2] G. Forman, "An extensive empirical study of feature selection metrics for text classification," *J. Mach. Learn. Res.*, vol. 3, pp. 1289–1305, 2003.
- [3] J. V. Haxby, M. I. Gobbini, M. L. Furey, A. Ishai, J. L. Schouten, and P. Pietrini, "Distributed and overlapping representations of faces and objects in ventral temporal cortex," *Science*, vol. 293, pp. 2425–2430, Sept. 2001.
- [4] A. M. Chan, E. Halgren, K. Marinkovic, and S. S. Cash, "Decoding word and category-specific spatiotemporal representations from MEG and EEG," *NeuroImage*, vol. 54, pp. 3028–3039, 2011.
- [5] S. Ryali, K. Supekar, D. A. Abrams, and V. Menon, "Sparse logistic regression for whole-brain classification of fMRI data," *NeuroImage*, vol. 51, pp. 752–764, 2010.
- [6] A. Gustafsson, A. Hermann, and F. Huber, *Conjoint Measurement: Methods and Applications*. Berlin: Springer-Verlag, 2007.
- [7] E. P. Xing, M. I. Jordan, and R. M. Karp, "Feature selection for high-dimensional genomic microarray data," in *Int'l Wkshp. Mach. Learn.*, pp. 601–608, 2001.
- [8] P. T. Boufounos and R. G. Baraniuk, "1-bit compressive sensing," in *Proc. Conf. Inform. Science & Sys.*, (Princeton, NJ), Mar. 2008.
- [9] Y. Plan and R. Vershynin, "Robust 1-bit compressed sensing and sparse logistic regression: A convex programming approach," in *arXiv: 1202.1212*, Feb. 2012.

[10] D. Koller and M. Sahami, "Toward optimal feature selection," in *Proc. 13th Int'l Conf. Machine Learning (ICML)* (L. Saitta, ed.), (Bari, Italy), pp. 284–292, 1996.

[11] R. Kohavi and G. John, "Wrapper for feature subset selection," *Artificial Intell.*, vol. 97, pp. 273–324, 1997.

[12] M. E. Tipping, "Sparse Bayesian learning and the relevance vector machine," *J. Mach. Learn. Res.*, vol. 1, pp. 211–244, 2001.

[13] M. Figueiredo, "Adaptive sparseness using Jeffreys' prior," in *Proc. 14th Conf. Advances Neural Inform. Process. Sys.*, pp. 697–704, MIT Press, Cambridge, MA, 2001.

[14] M. Figueiredo, "Adaptive sparseness for supervised learning," *IEEE Trans. Pattern Anal. Mach. Intell. (PAMI)*, vol. 25, no. 9, pp. 1150–1159, 2003.

[15] A. Kabán, "On Bayesian classification with Laplace priors," *Pattern Recognition Lett.*, vol. 28, no. 10, pp. 1271–1282, 2007.

[16] H. Chen, P. Tino, and X. Yao, "Probabilistic classification vector machines," *IEEE Trans. Neural Net.*, vol. 20, no. 6, pp. 901–914, 2009.

[17] G.-X. Yuan, K.-W. Chang, C.-J. Hsieh, and C.-J. Lin, "A comparison of optimization methods and software for large-scale L1-regularized linear classification," *J. Mach. Learn. Res.*, vol. 11, pp. 3183–3234, 2010.

[18] S. Rangan, "Generalized approximate message passing for estimation with random linear mixing," in *Proc. IEEE Int'l Symp. Inform. Theory*, (St. Petersburg, Russia), pp. 2168–2172, Aug. 2011. (Full version at [arXiv:1010.5141](https://arxiv.org/abs/1010.5141)).

[19] D. L. Donoho, A. Maleki, and A. Montanari, "Message passing algorithms for compressed sensing," in *Proceedings of the National Academy of Sciences*, vol. 106, pp. 18914–18919, Nov. 2009.

[20] D. L. Donoho, A. Maleki, and A. Montanari, "Message passing algorithms for compressed sensing: I. motivation and construction," in *Proc. of Information Theory Workshop*, Jan. 2010.

[21] A. Javanmard and A. Montanari, "State evolution for general approximate message passing algorithms, with applications to spatial coupling," [arXiv:1211.5164](https://arxiv.org/abs/1211.5164), Nov. 2012.

[22] J. Ziniel, S. Rangan, and P. Schniter, "A generalized framework for learning and recovery of structured sparse signals," in *Proc. IEEE Stat. Signal Process. Wkshp.*, (Ann Arbor, MI), Aug. 2012.

[23] J. P. Vila and P. Schniter, "Expectation-Maximization Gaussian-mixture approximate message passing," *IEEE Trans. Signal Process.*, vol. 61, pp. 4658–4672, Oct. 2013.

[24] B. J. Frey and D. J. C. MacKay, "A revolution: Belief propagation in graphs with cycles," *Adv. Neural Info. Process. Sys.*, pp. 479–485, 1998.

[25] F. R. Kschischang, B. J. Frey, and H. A. Loeliger, "Factor graphs and the sum-product algorithm," *IEEE Trans. Inform. Theory*, vol. 47, pp. 498–519, Feb. 2001.

[26] R. J. McEliece, D. J. C. MacKay, and J. Cheng, "Turbo decoding as an instance of Pearl's belief propagation algorithm," *IEEE J. Select. Areas Comm.*, vol. 16, pp. 140–152, Feb. 1998.

[27] W. T. Freeman, E. C. Pasztor, and O. T. Carmichael, "Learning low-level vision," *Int'l. J. Comp. Vision*, vol. 40, pp. 25–47, Oct. 2000.

[28] S. Rangan, P. Schniter, E. Riegler, A. K. Fletcher, and V. Cevher, "Fixed points of generalized approximate message passing with arbitrary matrices," in *Proc. IEEE Int'l Symp. Inform. Theory*, (Istanbul), July 2013. (Full version at [arXiv:1301.6295](https://arxiv.org/abs/1301.6295)).

[29] H.-A. Loeliger, "An introduction to factor graphs," *IEEE Signal Process. Mag.*, vol. 21, pp. 28–41, Jan. 2004.

[30] J. Ziniel, *Message Passing Approaches to Compressive Inference Under Structured Signal Priors*. PhD thesis, The Ohio State University, 2014.

[31] M. I. Jordan, "Why the logistic function? A tutorial discussion on probabilities and neural networks," 1995.

[32] C. E. Rasmussen and C. K. I. Williams, *Gaussian Processes for Machine Learning*. The MIT Press, 2006.

[33] J. Bi, K. Bennett, M. Embrechts, C. Breneman, and M. Song, "Dimensionality reduction via sparse support vector machines," *J. Mach. Learn. Res.*, vol. 3, pp. 1229–1243, 2003.

[34] M. Opper and O. Winther, *Gaussian Processes and SVM: Mean Field Results and Leave-One-Out Estimator*, ch. 17, pp. 311–326. MIT Press, 2000.

[35] P. Schniter, "Turbo reconstruction of structured sparse signals," in *Conf. on Information Sciences and Systems (CISS)*, (Princeton, NJ), pp. 1–6, Mar. 2010.

[36] H. Zou and T. Hastie, "Regularization and variable selection via the elastic net," *J. Roy. Statist. Soc., B*, vol. 67, no. 2, pp. 301–320, 2005.

[37] A. K. Nigam, K. and McCallum, S. Thrun, and T. Mitchell, "Text classification from labeled and unlabeled documents using EM," *Machine Learning*, vol. 39, pp. 103–134, 2000.

[38] J. P. Vila and P. Schniter, "An empirical-bayes approach to recovering linearly constrained non-negative sparse signals," [arXiv:1310.2806](https://arxiv.org/abs/1310.2806), Oct. 2013.

[39] A. P. Dempster, N. M. Laird, and D. B. Rubin, "Maximum likelihood from incomplete data via the EM algorithm," *J. Roy. Statist. Soc., B*, vol. 39, pp. 1–38, 1977.

[40] U. S. Kamilov, S. Rangan, A. K. Fletcher, and M. Unser, "Approximate message passing with consistent parameter estimation and applications to sparse learning," in *Proc. Neural Inform. Process. Syst. Conf.*, (Lake Tahoe, NV), Dec. 2012. (Full version at [arXiv:1207.3859](https://arxiv.org/abs/1207.3859)).

[41] S. Z. Li, *Markov Random Field Modeling in Image Analysis*. Springer-Verlag, 3rd ed., 2009.

[42] C. A. Bouman, K. Sauer, and S. Saquib, "Markov random fields and stochastic image models," in *IEEE Int'l. Conf. Image Process.*, 1995.

[43] S. Som and P. Schniter, "Approximate message passing for recovery of sparse signals with Markov-random-field support structure," in *Int'l Conf. Mach. Learn.*, (Bellevue, Wash.), Jul. 2011.

[44] J. Zhang, "The mean field theory in EM procedures for Markov random fields," *IEEE Trans. Signal Process.*, vol. 40, no. 10, pp. 2570–2583, 1992.

[45] D. D. Lewis, Y. Yang, T. G. Rose, and F. Li, "RCV1: A new benchmark collection for text categorization research," *J. Mach. Learn. Res.*, vol. 5, pp. 361–397, 2004.

[46] C. Lin, R. C. Weng, and S. S. Keerthi, "Trust region Newton methods for large-scale logistic regression," in *Proc. 24th Int'l Conf. Mach. Learn.*, (Corvallis, OR), pp. 561–568, 2007.

[47] S. R. Becker, E. J. Candès, and M. C. Grant, "Templates for convex cone problems with applications to sparse signal recovery," *Math. Prog. Comp.*, vol. 3, no. 3, pp. 165–218, 2011.

[48] C. J. Lin and J. J. Moré, "Newton's method for large-scale bound constrained problems," *SIAM J. Optimization*, vol. 9, pp. 1100–1127, 1999.

[49] P. Schniter and S. Rangan, "Compressive phase retrieval via generalized approximate message passing," in *Allerton Conf. on Commun., Control, and Comput.*, (Monticello, IL), Oct. 2012.

[50] K. A. Norman, S. M. Polyn, G. J. Detre, and J. V. Haxby, "Beyond mind-reading: multi-voxel pattern analysis of fMRI data," *Trends in Cognitive Sciences*, vol. 10, pp. 424–430, Sep. 2006.

[51] F. Pereira, T. Mitchell, and M. Botvinick, "Machine learning classifiers and fMRI: A tutorial overview," *NeuroImage*, vol. 45, pp. S199–S209, Mar. 2009.

[52] A. J. O'Toole, F. Jiang, H. Abdi, N. Penard, J. P. Dunlop, and M. A. Parent, "Theoretical, statistical, and practical perspectives on pattern-based classification approaches to functional neuroimaging analysis," *J. Cognitive Neurosci.*, vol. 19, pp. 1735–1752, 2007.

[53] M. de Brecht and N. Yamagishi, "Combining sparseness and smoothness improves classification accuracy and interpretability," *NeuroImage*, 2012.

[54] D. R. Barr and E. T. Sherrill, "Mean and variance of truncated normal distributions," *American Statistician*, vol. 53, Nov. 1999.